ACS NANO
Cite This: ACS Nano XXXX, XXX, XXX−XXX
www.acsnano.org

ARTICLE

Temperature-Induced Self-Compensating Defect Traps and Gain Thresholds in Colloidal Quantum Dots

Randy P. Sabatini,[†] Golam Bappi,[†] Kristopher T. Bicanic, Fengjia Fan, Sjoerd Hoogland, Makhsud I. Saidaminov, Laxmi K. Sagar, Oleksandr Voznyy, and Edward H. Sargent*

Department of Electrical and Computer Engineering, University of Toronto, 10 King's College Road, Toronto, Ontario M5S 3G4, Canada

Supporting Information

ABSTRACT: **Continuous-wave (CW) lasing was recently achieved in colloidal quantum dots (CQDs) by lowering the threshold through the introduction of biaxial strain. However, the CW laser threshold is still much higher than the femtosecond threshold. This must be addressed before electrically injected lasing can be realized. Here we investigate the relationship between threshold and temperature and find a subpicosecond recombination process that proceeds very efficiently at temperatures reached during CW excitation. We combine density functional theory and molecular dynamics simulations to explore potential candidates for such a process, and find that crystal defects having thermally vibrating energy levels can become electronic traps—*i.e.*, they can protrude into the bandgap—when they are sufficiently distorted at higher temperatures. We find that biaxially strained CQDs, which have a lower femtosecond laser threshold than traditional CQDs, result in less heat for a given transparency/gain level and thus undergo this trapping to a lower extent. We also propose methods to tailor CQDs to avoid self-compensating defect traps.**

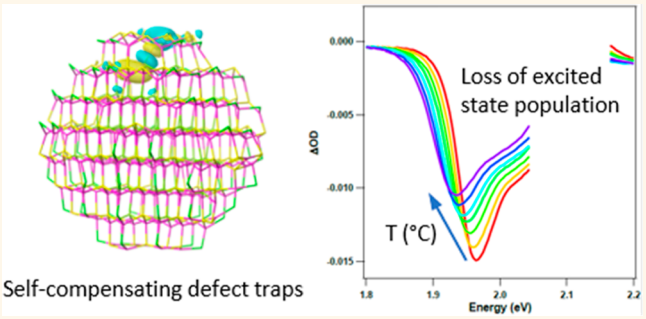

KEYWORDS: *colloidal quantum dots, optical gain, amplified spontaneous emission, trapping, temperature dependence, CdSe, p-doping*

Optical gain was observed in colloidal quantum dots in 2000.[1] For over a decade, however, CQD lasing was limited to nanosecond operation.[2−4] Longer duration pulses heat the sample and lead to thermal damage. Lasing in the microsecond regime was achieved by increasing the compactness of the CQD film and raising the thermal conductivity of the substrate, working against heat buildup in the sample.[5]

For CW operation, the threshold needed to be lowered further to allow CW photoexcitation without damage to the film.[6] In conventional CdSe-based CQDs, degeneracy of the valence band energy levels militates against this effort: while the conduction band-edge of CdSe CQDs contains a singly degenerate, s-character electron level, the valence band contains four closely spaced hole levels,[7,8] each 2-fold degenerate due to spin. If these eight hole levels are close to being degenerate, more excitons are needed to achieve population inversion.

To lower the degeneracy, asymmetric shapes have been employed, including quantum dots in rods, nanoplatelets, and biaxially strained CQDs.[6,9,10] Femtosecond optical gain measurements revealed that CdSe/CdS core/shell CQDs with a built-in biaxial strain had ∼1.4× lower thresholds than traditionally grown CQDs with similar core sizes, shell thicknesses, and photoluminescence quantum yields. However, this effect was magnified during CW photoexcitation, and only the biaxially strained CQDs were able to reach the threshold before burning. Quasi-CW photoexcitation (∼30 μs) of traditional dots led to a threshold ∼3× higher than that of biaxially strained CQDs.[6]

Herein, we account for the CW threshold deterioration in the context of the temperature dependence of the excited-state depopulation. While quantum dots have been investigated in different temperature ranges,[9,11−15] few studies extend this to above 50 °C, temperatures high enough to be relevant for laser operation under CW excitation.[13−15] We investigate the temperature dependence of biaxially and hydrostatically strained CQDs in the 20−140 °C range in order to quantify

Received: April 12, 2019
Accepted: July 16, 2019
Published: July 16, 2019

DOI: 10.1021/acsnano.9b02834
ACS Nano XXXX, XXX, XXX−XXX

the effect of temperature on its excited-state properties. In particular, we identify and investigate an ultrafast (sub-350 fs) electron-trapping process that is activated by temperature and has a superlinear effect on gain threshold in the CW regime. We term this process self-compensating defect trapping.

RESULTS AND DISCUSSION

Hydrostatically and biaxially strained CQDs were grown according to the literature.[6] In the synthesis of biaxially strained CQDs, biaxial strain was introduced using a two-step shell growth process.[6] We began with an asymmetric wurtzite crystal structure for CdSe with weakly binding oleylamine as ligand. The first CdS shell was grown using the sulfur source trioctylphosphine sulfide (TOPS). TOPS in the presence of competing amines becomes facet-selective, enabling asymmetric growth in a disklike structure having an off-center core (Figure 1a). This shape asymmetry induces biaxial strain that,

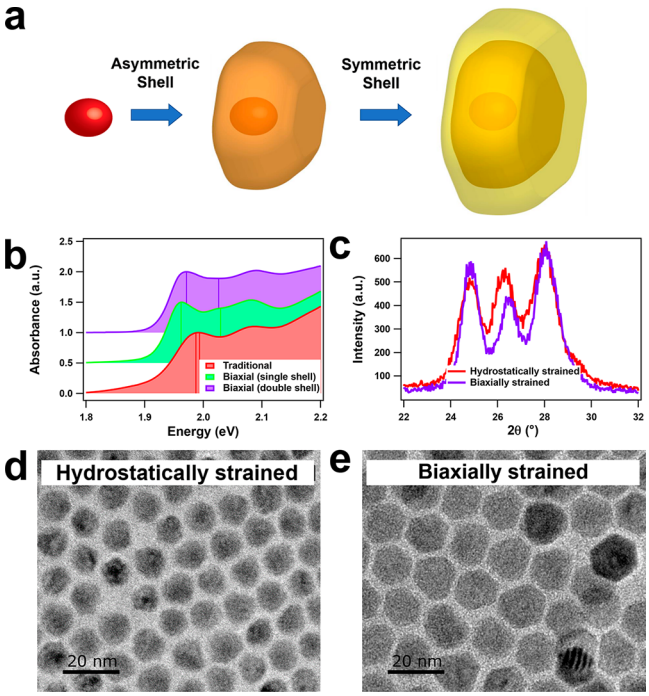

Figure 1. Synthesis of biaxially strained CQDs that lead to increased splitting among valence band levels. (a) Stepwise shell growth, where an asymmetric shell is grown first and then a symmetric shell is grown atop. (b) Absorption spectra of conventional *vs* biaxially strained CQDs in solution, with lines showing the splitting of valence band-edge states due to biaxial strain. (c) XRD of hydrostatically and biaxially strained CQDs. The shift of only the (002) peak can be explained from the observation that biaxial strain is indeed present. TEM images of (d) conventional (hydrostatically strained) and (e) biaxially strained CQDs.

in turn, lowers the overall degeneracy of the system by increasing the separation among valence band-edge states. As a result of this splitting, an extra peak is resolved in the linear absorption spectrum (Figure 1b). A second, more symmetric, shell is then grown to passivate further the CQDs. While the second shell broadens the absorption features, its addition nevertheless retains the desired splitting, thus maintaining the extra absorption peak (Figure 1b).

The presence of an asymmetric shell has previously been confirmed using energy-dispersive X-ray spectroscopy, and high-resolution TEM imaging verified that asymmetric strain was present.[6] XRD measurements (Figure 1c) similarly confirm the presence of this asymmetric strain, given the shift of only the (002) peak relative to conventional hydrostatically strained CQDs. While alloying of CdSe and CdS has also been shown to split the fundamental absorption peak of CdSe,[16] we ruled out the possibility that it occurs during the first shell growth stage because the band-edge absorption does not blue-shift, a phenomenon commonly observed when core and shell intermix. Additionally, alloying usually requires the introduction of mixed S−Se precursors, whereas we grow the CdS shells on top of the preformed CdSe cores.

To isolate material properties without influence from cavity effects, we chose to investigate film-amplified spontaneous emission (ASE), rather than lasing. We first performed temperature-dependent linear absorption spectroscopy (Figure S1a,b) to determine the appropriate photoexcitation wavelengths. In the linear absorption spectra, the absorbance remains unchanged (isosbestic point) for all temperatures at 2.09 eV (592 nm) for both biaxially and hydrostatically strained CQDs, respectively; these wavelengths were used therefore in photoexciting the samples for all spectroscopic experiments to normalize the photons absorbed for each temperature. All changes measured in the optical properties were confirmed to be reversible (Figure S2a−f) after the CQD films were heated to 140 °C. The reversibility of optical properties was previously shown for CdSe/ZnS core/shell CQDs even after annealing to ∼327 °C, and irreversibility after heating to higher temperatures was attributed to loss of particle integrity.[15]

We then measured the effect of temperature on the amplified spontaneous emission (ASE) threshold using a ∼250 fs source at the linear absorption isosbestic points. For each temperature, we observed—when we increased the photoexcitation power—a photoluminescence increase (Figure S3). After the threshold was reached, a narrower peak emerged, consistent with amplified spontaneous emission. For both samples, the ASE peak red-shifts as a function of temperature by ∼0.2 meV/K (Figure 2a). Their thresholds increase with temperature at a rate of ∼3 $\mu J/cm^2/K$ in both samples (Figure 2b). Compared to traditional quantum dots, biaxially strained CQDs exhibit a ∼ 1.4x lower threshold, which translates into proportionately lower thresholds even at elevated temperatures. We have ruled out effects from film morphology and self-absorption (Figure S4−5) and instead attribute this threshold lowering to the difference in degeneracy. For comparison, the fs ASE threshold for biaxially strained CQDs at ∼95 °C is the same as the threshold for traditional CQDs at room temperature. Furthermore, at room temperature, the lower threshold of biaxially strained CQDs means they achieve ASE at much lower excitation fluxes, avoiding the buildup of heat.

To explore the effect on transient heating of longer duration pulses, we simulated the temperature of a ∼200 nm CQD thin film on a magnesium fluoride substrate under 2.81 eV photoexcitation. The heat generation is due both to Auger recombination (previously estimated at 80% of input excitation power)[6] and to thermalization (difference in energy between the excitation and emission). The thermal simulations show the resulting nonlinear increase in CQD film temperature with

DOI: 10.1021/acsnano.9b02834
ACS Nano XXXX, XXX, XXX−XXX

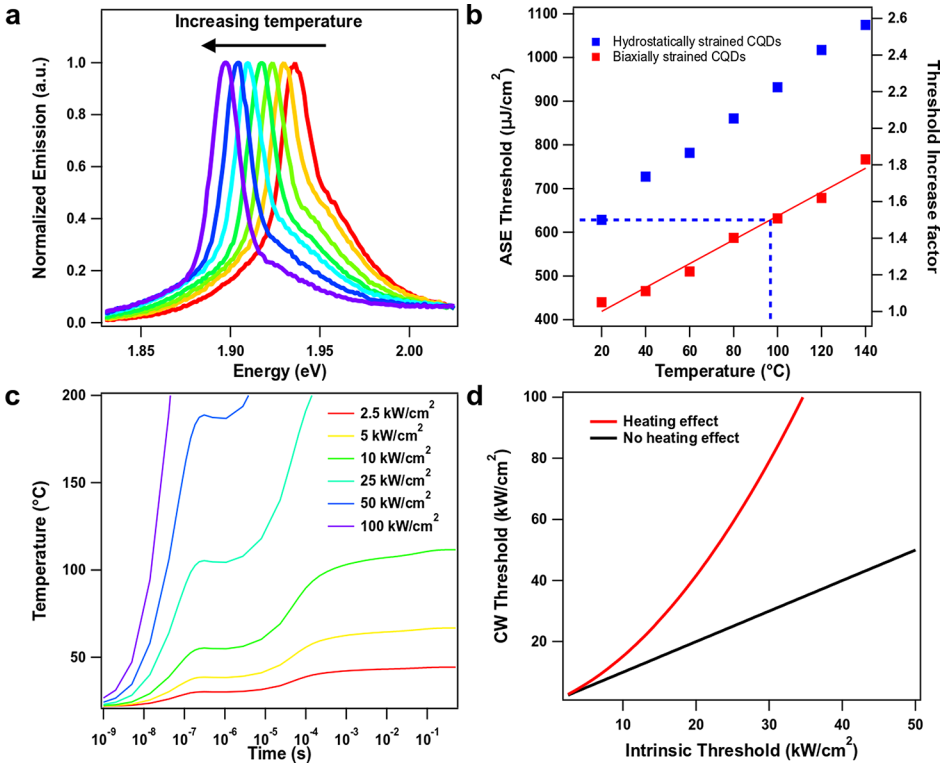

Figure 2. Temperature dependence of amplified spontaneous emission. (a) Temperature-dependent ASE spectra. (b) Temperature-dependent ASE thresholds of biaxially strained CQDs, compared to that of traditional CQDs. The ASE thresholds were confirmed to be reversible after heating the films to 140 °C. (c) Temperature increase as a function of pulse duration for increasing pump powers, assuming 80% conversion to heat *via* Auger recombination. (d) Dependence of the CW threshold, based on the intrinsic threshold. Heating occurs due to the thermalization and Auger recombination, which decreases the efficiency.

respect to absorbed power (Figure 2c). For each power, the temperature rises with pulse duration until the system reaches equilibrium—this is the temperature of the system under CW illumination. For comparison, the emission of a CQD film pulsed at 300 ns will differ from one photoexcited under CW conditions (Figure S6). Knowing the threshold increase with temperature (from Figure 2b), we can estimate the true threshold under CW pumping (Figure 2d). The data show a superlinear increase in CW thresholds *vs* fs-pulsed threshold due to the heating effect. Conversely, lowering the intrinsic threshold (*e.g.*, by lowering the degeneracy) will cause a superlinear decrease in the CW threshold (with respect to the intrinsic fs threshold).

While the overall ASE threshold is better for biaxially strained CQDs, the thresholds for both do increase by a similarly large amount (~2×) within this temperature range. Additionally, the quantum yields are affected by temperature as well. We measured temperature-dependent steady-state emission of both biaxially and hydrostatically strained CQDs (Figures 3a,b). The emission peaks red-shift by ~0.3 meV/K, and the emission intensity decreases at higher temperatures. We integrated the emission at different temperatures to determine that the relative quantum yields decrease by about 60% from 20 to 140 °C for both types of CQDs (Figures 3c,d).

To gain insight into these large changes, we utilized ultrafast transient absorption spectroscopy and compared the results obtained from linear absorption (Figure 4). Spectra at a time delay of 25 ps were monitored at different temperatures. This time delay is early enough to avoid the effects of biexciton Auger recombination, with Auger lifetimes >350 ps at all temperatures (Figures S7 and S8). No faster time constants were resolvable (Figure S9) within our instrument response (~350 fs). In addition, the long-time constant appears to be unchanged as the temperature is increased (Figure S8).

However, for both conventional and biaxially strained CQDs, we observe that the ground-state bleach amplitude at the earliest observed times decreases by ~30% and 50% upon heating to 140 °C (Figure 4b,d), respectively, much larger than the change observed in linear absorption (Figure 4a,c). This suggests that, upon excitation, the number of excited photocarriers significantly decreases within the instrument response of the experiment (~350 fs). We assign electrons as the participating photocarrier (SI Note 1). Previous studies[14] on CQDs found that increased temperatures resulted in lower gain, and biexciton Auger was assumed to lead to nonradiative losses through additional heating. However, here we clearly observe ultrafast carrier loss at very low pump fluences which is highly temperature sensitive. We show further that this effect can be observed in CQDs capped with Cl^- ligands, showing that this loss is not ligand-specific (Figure S10).

We have also analyzed the effect of higher energy states on the ground-state bleach to test whether thermal depopulation could affect it or if another mechanism is responsible. We note that the second bleach arises from the same band-edge electron state and a deeper hole state. Population of this electron state is practically unaffected by temperature since the next electron state is ~100 meV higher in energy.[6] Thus, the first and the second bleach show essentially the same amplitude change, and their convolution does not affect our estimate of the bleach decrease. Our numerical simulations using thermal

DOI: 10.1021/acsnano.9b02834
ACS Nano XXXX, XXX, XXX−XXX

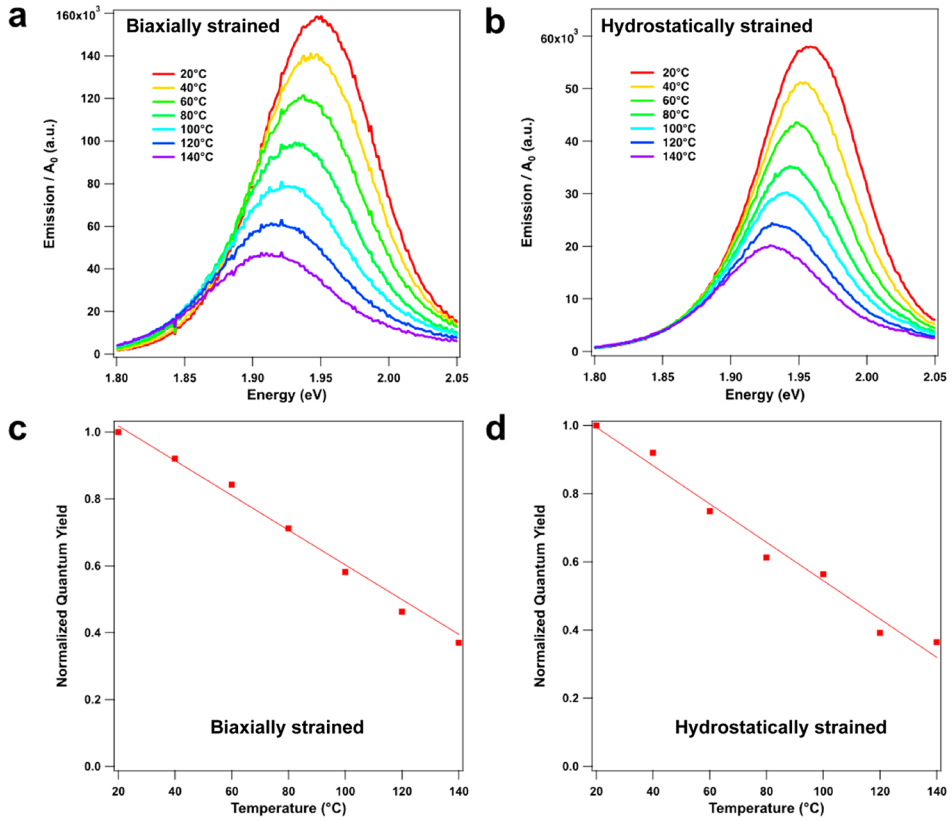

Figure 3. Temperature-dependent emission. Temperature-dependent emission spectra for (a) biaxially strained and (b) hydrostatically strained CQDs. Relative photoluminescence quantum yields for (c) biaxially strained and (d) hydrostatically strained CQDs as a function of temperature. The film PLQYs at 20 °C for both samples lie between 35 and 40%.

distribution and accounting for hole state splitting revealed that thermal repopulation of higher levels would account for at most 7% of this decrease[6] (details in Table S1). Most of the bleach decrease is thus caused by another factor.

The TA measurements point to a subpicosecond process that depopulates the excited state. Subpicosecond trapping assisted by an Auger cooling process (*i.e.*, not requiring a biexciton) has been previously predicted theoretically.[17,18] Experimentally, electron trapping in CdTe has been shown to occur on a subpicosecond time scale, also ascribed to an Auger cooling process.[19] In that study, ultrafast transient absorption spectroscopy was used to probe the excited-state population, and the ground-state bleach was found to increase with an applied negative bias. This bias filled the trap states, preventing their interaction with excited carriers.

In our experiments, however, we observe a loss of excited-state population at higher temperatures, and we propose a contribution from phonons to be the cause. Midgap states require phonons to couple to the conduction or valence band edge in order to trap electrons. Often, traps levels are thought of as static, where virtual phonons allow transfer of charges. Alternatively, in a real-space picture, the trap energy levels vibrate, and these vibrations become more pronounced with increasing temperatures. Larger vibrations can eventually lead to traps overlapping with the conduction or valence bands. It should be noted that trapping, *i.e.*, electron transfer, between a bandedge and a trap state, does not necessarily require the states to be in resonance. Transfer probability over an energy gap increases if the state's wave function changes dramatically over time.[20]

The origin of the defects in CdSe CQDs still remains a subject of scientific investigation. Cd oleate vacancies on the surface exposing Se dangling bonds were shown to degrade PL significantly.[21,22] However, here we need a less efficient trap that could, however, exhibit temperature dependence. We started our search from the knowledge that CdSe CQDs are impossible to *p*-dope, even when an ambient environment induces oxidation: this effect is called self-compensation, *i.e.*, the formation of defects in response to doping,[23] and is also well-known in bulk CdSe. However, the self-compensating defects in CQDs could potentially be different from those in bulk due to the abundance of surfaces in CQDs.

We thus constructed, in simulations, a defect-free CQD (Figure 5a), *p*-doped it, and evolved it through a sufficiently long molecular dynamics run. We observed a facile formation of Se dimers on the CQD surface as a form of self-compensation. The Se atom on the surface sinks into the subsurface, breaking the bond to a Cd and forming a bond to a subsurface Se, restoring the charge balance (Figure 5b). Similar defects are formed in CdS-terminated CQDs. Using static density functional theory (DFT) calculations, we find the surface S and Se dimers are 0.45 and 0.32 eV more stable than the nondefected structure under *p*-doped condition, respectively, whereas the Se dimer inside the core is 0.9 eV less stable than the nondefected structure. Se and S dimers levels lie close to the conduction bandedge, but inside the conduction band, and thus are not traps in the static configuration or at low temperatures (Figure 5c). At high temperatures, however, these levels vibrate sufficiently to enter the bandgap (Figure 5d) and thus are likely to participate in electron trapping. We

DOI: 10.1021/acsnano.9b02834
ACS Nano XXXX, XXX, XXX−XXX

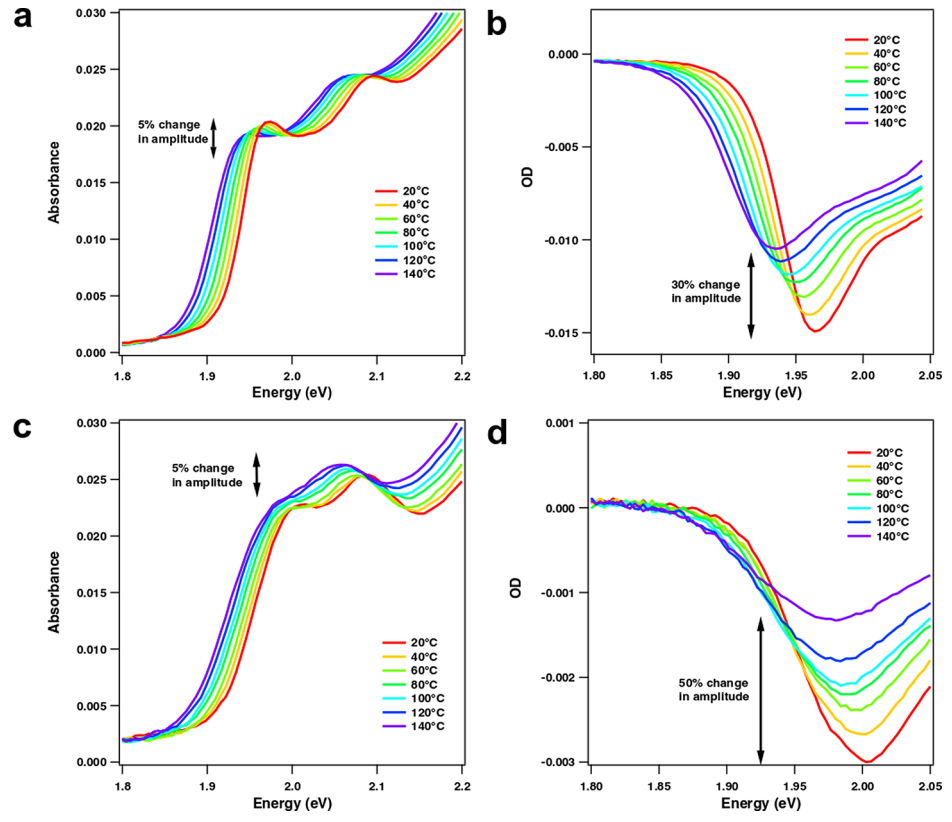

Figure 4. Temperature dependence of linear and transient absorption: (a) Temperature-dependent linear absorption spectra of biaxially strained CQDs. (b) Ultrafast transient absorption spectra following a 25 ps delay, as a function of temperature, for biaxially strained CQDs. (c) Temperature-dependent linear absorption spectra of hydrostatically strained CQDs. (d) Ultrafast transient absorption spectra following a 25 ps delay, as a function of temperature, for hydrostatically strained CQDs.

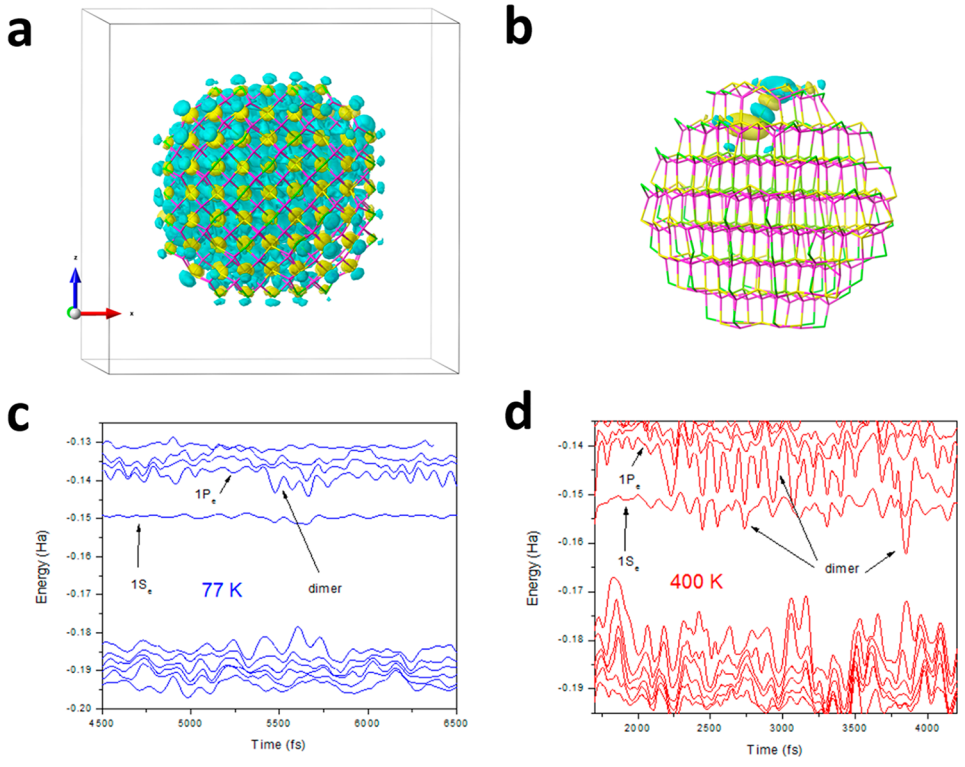

Figure 5. Trapping simulations: (a) defect-free CQD, (b) dimer on CQD surface, a result of self-compensation, (c) molecular dynamics of the CQD at 77 K, (d) molecular dynamics of the CQD at 400 K.

DOI: 10.1021/acsnano.9b02834
ACS Nano XXXX, XXX, XXX−XXX

find Se dimers to locate closer to the bandedge and are thus more easily activated with temperature. Nevertheless, at sufficiently high temperatures, S dimers in CdSe/CdS core−shell CQDs become traps and can capture electrons from the core, which are known to delocalize into the shell. We term this process self-compensating defect trapping.

In summary, CW excitation causes a temperature increase, which results in dynamic activation of traps, leading to highly efficient depopulation of excited electrons. Utilization of biaxially strained CQDs helps to mitigate this effect under CW excitation even though the energetics of trap activation is not affected. Instead, the lower inherent threshold for biaxially strained CQDs results in much less heat build-up.

Looking forward, we propose that next generations of CQDs will be called upon to address these self-compensating defect traps. While lowering the threshold is still desired, progress must be made toward limiting the effects of increased temperature. Specifically, oxidation (*i.e.*, *p*-doping) must be avoided, as this leads to the formation of Se and S dimers; these dimers effectively trap electrons at raised temperatures. We posit that variable oxidation state dopants may be one method to overcome this issue. Based on our simulations (Figure 2D), we expect laser thresholds to be lowered by up to an order of magnitude.

CONCLUSIONS

We have analyzed the effects of temperature on gain characteristics in biaxially and hydrostatically strained CQDs. We find that increased temperatures introduce a subpicosecond self-compensating defect trapping, which greatly reduces the excited state population. We have combined experiments and theory to investigate the cause of this trapping process, which we attribute to dimer formation on the surface. Compared to conventional CQDs, the use of biaxially strained CQDs allows a lower threshold, which causes less heat build-up within the sample. This can mitigate the effect of the electron trapping process, increasing their performance in lasing applications.

EXPERIMENTAL METHODS

Synthesis. Biaxially strained and traditional core−shell CdSe/CdS quantum dots were synthesized according to literature.[6] Chloride exchanged quantum dots were synthesized according to literature. Films were prepared by spin-coating a concentrated solution of CQDs onto glass slides.

Heating Setup. The sample was taped onto a silver mirror, which was housed in an aluminum block with a resistive heater. Active feedback was controlled using a thermocouple and a temperature controller.

Linear Absorption. Linear absorption spectra were measured with a PerkinElmer Lambda 950 UV/vis/NIR spectrophotometer, using an integrating sphere. The sample, mounted on the temperature controller, was placed directly outside a port on the integrating sphere, and the spectra were taken with no ambient lighting. Absorption spectra were also measured using a bare glass slide with the temperature controller and were used as baselines for each temperature.

Steady-State Emission. Photoluminescence spectra were collected with an Ocean Optics USB 2000+ spectrometer using both a 592 nm fs laser source (see transient absorption section) and the 500 nm emission of a xenon lamp. Relative photoluminescence quantum yields were calculated by integrating the emission at different temperatures.

Transient Absorption Spectroscopy. A Yb:KGW regenerative amplifier (Pharos, Light Conversion) produced the 1030 nm fundamental (5 kHz). A portion of the beam was passed through an optical parametric amplifier (Orpheus, Light Conversion) to generate the 2.09 eV pump pulse. Both the pump pulse and residual fundamental were sent into an optical bench (Helios, Ultrafast). The fundamental was sent through a delay stage, which determines the time delay between the two pulses, and then was focused into a sapphire crystal, generating a white light continuum. The pump pulse was sent through an optical chopper, reducing its frequency to 2.5 kHz. Both beams were then focused onto the sample. The probe light reflected off the mirror and was directed toward a CCD (Helios, Ultrafast).

ASE Measurements. With the laser from the transient absorption setup, the sample was illuminated with a spot of 2.09 eV light at different powers. Emitted light was collected using a USB 2000+ spectrometer.

SES Measurements. Light with wavelength 355 nm from a 1 ns pulsed laser was used. A 25.4 mm focal length circular lens was used to focus the beam to a spot. The emission was collected from the edge using a multimode fiber and coupled into a USB 2000+ spectrometer.

Imaging. Images were taken with an optical microscope (Nikon Eclipse LV100). Atomic force microscopy measurements were performed with an Asylum Research Cypher S operating in alternating-current contact mode.

Numerical Model. This was based on a previous model[6] and includes degeneracy, inhomogeneous broadening, oscillator strengths of transitions, biexciton binding energy, and temperature. Based on 4 (doubly degenerate for spin) hole states, and 1 (spin-degenerate) electron level we obtain 16 exciton states of varying levels of brightness, following our previous results.[6] See Table S1 for model parameters.

Thermal Simulations. ANSYS simulation software package was used for modeling the transient thermal response of our colloidal quantum dot film under a continuous excitation source. The colloidal quantum dot (CQD) films with a thickness of 200 nm were analyzed on a thermally conductive, optically transparent, substrate with an excitation spot size of 50 μm × 30 μm. The heat generation that was implemented in this volume was calculated based on heat generated by quantum defect (thermalized energy from the energy difference between the higher energy excitation and the lower energy emission) in addition to the thermal heat generated by Auger recombination. The MgF_2 substrate was created to be bulklike to ensure it would act as a heat sink, resembling operation in a device. In addition to this, the rear side of the MgF_2 was held at 295 K. We allowed the simulation to evolve in time until the sample's temperature had saturated, where we reported the maximum temperature in the CQD film in the excitation spot center. Heat generation of 1.28×10^{15} W/m^3 was used, taking into account the quantum yield and quantum defect, both of which lead to heat generation. Heat constants of quantum dots were taken from ref 5. See Table S2 for material properties used for thermal simulations.

ASSOCIATED CONTENT

Supporting Information

The Supporting Information is available free of charge on the ACS Publications website at DOI: 10.1021/acsnano.9b02834.

Tables showing parameters of model for numerical simulations and material properties used for thermal simulations. Figures showing lifetime of biexciton Auger recombination, temperature-dependent photoluminescence and linear absorption, emission with different excitation pulse lengths, power-dependent photoluminescence, temperature-dependent Auger recombination, and surface morphology studies (PDF)

AUTHOR INFORMATION

Corresponding Author

*E-mail: ted.sargent@utoronto.ca.

DOI: 10.1021/acsnano.9b02834
ACS Nano XXXX, XXX, XXX−XXX

ORCID

Randy P. Sabatini: 0000-0002-5975-4347
Kristopher T. Bicanic: 0000-0002-3020-4093
Oleksandr Voznyy: 0000-0002-8656-5074
Edward H. Sargent: 0000-0003-0396-6495

Author Contributions

[†]R.P.S. and G.B. contributed equally to this work.

Notes

The authors declare no competing financial interest.

ACKNOWLEDGMENTS

This publication is based in part on the work supported by the Ontario Research Fund - Research Excellence Program and by the Natural Sciences and Engineering Research Council (NSERC) of Canada. M.I.S. acknowledges the Government of Canada's Banting Postdoctoral Fellowship Program for financial support. Partial support was provided by Christie Digital Systems Canada. We thank D. Kopilovic for discussions during this work.

REFERENCES

(1) Klimov, V. I.; Mikhailovsky, A. A.; Xu, S.; Malko, A. A.; Hollingsworth, J. A.; Leatherdale, C. A.; Eisler, H. J.; Bawendi, M. G. Optical Gain and Stimulated Emission in Nanocrystal Quantum Dots. *Science* **2000**, *290*, 314−317.

(2) Chen, Y.; Herrnsdorf, J.; Guilhabert, B.; Zhang, Y.; Watson, I. M.; Gu, E.; Laurand, N.; Dawson, M. D. Colloidal Quantum Dot Random Laser. *Opt. Express* **2011**, *19*, 2996−3003.

(3) Guilhabert, B.; Foucher, C.; Haughey, A.-M.; Mutlugun, E.; Gao, Y.; Herrnsdorf, J.; Sun, H. D.; Demir, H. V.; Dawson, M. D.; Laurand, N. Nanosecond Colloidal Quantum Dot Lasers for Sensing. *Opt. Express* **2014**, *22*, 7308−7319.

(4) Schäfer, J.; Mondia, J. P.; Sharma, R.; Lu, Z. H.; Susha, A. S.; Rogach, A. L.; Wang, L. J. Quantum Dot Microdrop Laser. *Nano Lett.* **2008**, *8*, 1709−1712.

(5) Adachi, M. M.; Fan, F.; Sellan, D. P.; Hoogland, S.; Voznyy, O.; Houtepen, A. J.; Parrish, K. D.; Kanjanaboos, P.; Malen, J. A.; Sargent, E. H. Microsecond-Sustained Lasing from Colloidal Quantum Dot Solids. *Nat. Commun.* **2015**, *6*, 1−8.

(6) Fan, F.; Voznyy, O.; Sabatini, R. P.; Bicanic, K. T.; Adachi, M. M.; McBride, J. R.; Reid, K. R.; Park, Y. S.; Li, X.; Jain, A.; Quintero-Bermudez, R.; Saravanapavanantham, M.; Liu, M.; Korkusinski, M.; Hawrylak, P.; Klimov, V. I.; Rosenthal, S. J.; Hoogland, S.; Sargent, E. H. Continuous-Wave Lasing in Colloidal Quantum Dot Solids Enabled by Facet-Selective Epitaxy. *Nature* **2017**, *544*, 75−79.

(7) Franceschetti, A.; Fu, H.; Wang, L. W.; Zunger, A. Many-Body Pseudopotential Theory of Excitons in InP and CdSe Quantum Dots. *Phys. Rev. B: Condens. Matter Mater. Phys.* **1999**, *60*, 1819−1829.

(8) Korkusinski, M.; Voznyy, O.; Hawrylak, P. Fine Structure and Size Dependence of Exciton and Biexciton Optical Spectra in CdSe Nanocrystals. *Phys. Rev. B* **2010**, *82*, 1−16.

(9) Moreels, I.; Rainò, G.; Gomes, R.; Hens, Z.; Stöferle, T.; Mahrt, R. F. Nearly Temperature-Independent Threshold for Amplified Spontaneous Emission in Colloidal CdSe/CdS Quantum Dot-in-Rods. *Adv. Mater.* **2012**, *24*, 231−235.

(10) She, C.; Fedin, I.; Dolzhnikov, D. S.; Dahlberg, P. D.; Engel, G. S.; Schaller, R. D.; Talapin, D. V. Red, Yellow, Green, and Blue Amplified Spontaneous Emission and Lasing Using Colloidal CdSe Nanoplatelets. *ACS Nano* **2015**, *9*, 9475−9485.

(11) Brovelli, S.; Schaller, R. D.; Crooker, S. A.; García-Santamaría, F.; Chen, Y.; Viswanatha, R.; Hollingsworth, J. A.; Htoon, H.; Klimov, V. I. Nano-Engineered Electron-Hole Exchange Interaction Controls Exciton Dynamics in Core-Shell Semiconductor Nanocrystals. *Nat. Commun.* **2011**, *2*, 1−8.

(12) Jing, P.; Zheng, J.; Ikezawa, M.; Liu, X.; Lv, S.; Kong, X.; Zhao, J.; Masumoto, Y. Temperature-Dependent Photoluminescence of CdSe-Core CdS/CdZnS/ZnS-Multishell Quantum Dots. *J. Phys. Chem. C* **2009**, *113*, 13545−13550.

(13) Kalytchuk, S.; Zhovtiuk, O.; Kershaw, S. V.; Zbořil, R.; Rogach, A. L. Temperature-Dependent Exciton and Trap-Related Photoluminescence of CdTe Quantum Dots Embedded in a NaCl Matrix: Implication in Thermometry. *Small* **2016**, *12*, 466−476.

(14) Kazes, M.; Oron, D.; Shweky, I.; Banin, U. Temperature Dependence of Optical Gain in CdSe/ZnS Quantum Rods. *J. Phys. Chem. C* **2007**, *111*, 7898−7905.

(15) Rowland, C. E.; Schaller, R. D. Exciton Fate in Semiconductor Nanocrystals at Elevated Temperatures: Hole Trapping Outcompetes Exciton Deactivation. *J. Phys. Chem. C* **2013**, *117*, 17337−17343.

(16) Mourad, D.; Guille, A.; Aubert, T.; Brainis, E.; Hens, Z. Random-Alloying Induced Signatures in the Absorption Spectra of Colloidal Quantum Dots. *Chem. Mater.* **2014**, *26*, 6852−6862.

(17) Gómez-Campos, F. M.; Califano, M. Hole Surface Trapping in CdSe Nanocrystals: Dynamics, Rate Fluctuations, and Implications for Blinking. *Nano Lett.* **2012**, *12*, 4508−4517.

(18) Califano, M.; Gómez-Campos, F. M. Universal Trapping Mechanism in Semiconductor Nanocrystals. *Nano Lett.* **2013**, *13*, 2047−2052.

(19) Boehme, S. C.; Azpiroz, J. M.; Aulin, Y. V.; Grozema, F. C.; Vanmaekelbergh, D.; Siebbeles, L. D. A.; Infante, I.; Houtepen, A. J. Density of Trap States and Auger-Mediated Electron Trapping in CdTe Quantum-Dot Solids. *Nano Lett.* **2015**, *15*, 3056−3066.

(20) Akimov, A. V.; Prezhdo, O. V. The PYXAID Program for Non-Adiabatic Molecular Dynamics in Condensed Matter Systems. *J. Chem. Theory Comput.* **2013**, *9*, 4959−4972.

(21) Anderson, N. C.; Hendricks, M. P.; Choi, J. J.; Owen, J. S. Ligand Exchange and the Stoichiometry of Metal Chalcogenide Nanocrystals: Spectroscopic Observation of Facile Metal-Carboxylate Displacement and Binding. *J. Am. Chem. Soc.* **2013**, *135*, 18536−18548.

(22) Houtepen, A. J.; Hens, Z.; Owen, J. S.; Infante, I. On the Origin of Surface Traps in Colloidal II-VI Semiconductor Nanocrystals. *Chem. Mater.* **2017**, *29*, 752−761.

(23) Zunger, A. Practical Doping Principles. *Appl. Phys. Lett.* **2003**, *83*, 57−59.

DOI: 10.1021/acsnano.9b02834
ACS Nano XXXX, XXX, XXX−XXX